Solid-State Oxygen-17 Nuclear Magnetic Resonance Spectroscopic Studies of Zeolites and Related Systems. 2[§]

Hye Kyung C. Timken,[†] Nathan Janes,[†] Gary L. Turner,[†] Susan L. Lambert,[‡] L. B. Welsh,[‡] and Eric Oldfield*[†]

Contribution from the School of Chemical Sciences, University of Illinois at Urbana—Champaign, Urbana, Illinois 61801, and Signal Research Center, Inc., Des Plaines, Illinois 60017. *Received January 15, 1986*

Abstract: We have obtained solid-state ^{17}O NMR spectra of ^{17}O-enriched gallosilicates (gallium analogues of zeolite Na–X, sodalite, and Ba^{2+}-exchanged sodalite) and the porous aluminophosphates ($AlPO_4$-5, $AlPO_4$-11, and $AlPO_4$-17). The spectra yield nuclear quadrupole coupling constants (e^2qQ/h), electric field gradient tensor asymmetry parameters (η), and isotropic chemical shifts (δ_i) for the chemically distinct oxygens in the Si–O–Ga, Si–O–Si, and Al–O–P fragments. The e^2qQ/h values for these species, and for Si–O–Si and Si–O–Al in Na–A and Na–Y zeolites, are analyzed in terms of a Townes–Dailey theory, and the results are compared with the predictions of a previous wholly empirical approach (Schramm, S.; Oldfield, E. *J. Am. Chem. Soc.* **1984**, *106*, 2502). The results suggest that the empirical approach gives the best agreement between experiment and prediction when nonframework counterions are present (e.g., Si–O–Al, Si–O–Ga), but that the Townes–Dailey approximation yields the most accurate predictions in the absence of such species (e.g., Al–O–P).

There has recently been intense interest in studying zeolites and their porous aluminophosphate analogues by means of ^{27}Al, ^{29}Si, and ^{31}P NMR,[1-4] but only a brief mention of the ^{17}O NMR spectrum of a zeolite (Union Carbide A) has been made.[5] In our group, we have been applying ^{17}O solid-state NMR to study structure and bonding in a variety of oxides and silicates.[6,7] We have reported the first comprehensive investigation of the ^{17}O NMR of Na–A and Y zeolites by means of static, MASS (magic-angle sample-spinning) and VASS (variable-angle sample-spinning) techniques.[8] As an extension of our ^{17}O NMR investigation of zeolites, we present in this paper our recent results for gallosilicates (gallium analogues of zeolite X (Ga–X) and sodalites) and for several aluminophosphate materials ($AlPO_4$-5, $AlPO_4$-11, and $AlPO_4$-17). Our results indicate that the ^{17}O NMR spectra of these systems consist of resonances from chemically distinct oxygen species, Si[^{17}O]Si and Si[^{17}O]Ga for gallosilicates and Al[^{17}O]P for the $AlPO_4$ series. In addition, we have performed Townes–Dailey calculations for prediction of the nuclear quadrupole coupling constants, e^2qQ/h, and the asymmetry parameters, η, for each type of chemically nonequivalent oxygen observed in the zeolites, gallosilicates, and aluminophosphates, that is, Si[^{17}O]Si, Si[^{17}O]Al, Si[^{17}O]Ga, and Al[^{17}O]P. These results are compared with the experimental parameters, and with the predictions of a previous empirical correlation,[6] which related electronegativity and e^2qQ/h. The differences are discussed in terms of the likely coordination of oxygen by nonframework cations in the zeolites (and gallosilicates).

Experimental Section

Synthesis of [^{17}O] Sodium Zeolite Ga–X and Sodium Gallosodalite.[9] ^{17}O-Labeled zeolites were prepared by direct synthesis, incorporating $H_2{}^{17}O$ into the synthesis gel. The gallium analogues of Na–X and sodalite were synthesized using a slurry of composition $2.1Na_2O{\cdot}Ga_2O_3{\cdot}4SiO_2{\cdot}60H_2O$ and seeded with aluminosilicate seed materials (Union Carbide 13-X, 1% Al relative to gallium). Sodium hydroxide (1.68 g) was dissolved in 6.81 g of 20% ^{17}O-enriched water, and to this solution was added 1.874 g of gallium oxide. The mixture was stirred to dissolution. Next, Ludox HS-40 (6.01 g) and 0.12 g of aluminosilicate seed (13-X) were added with stirring. Two equal portions of the resultant gel were transferred into two 25-mL Parr bombs, which were aged 24 h, then autoclaved at 100 °C for 8 and 24 h, respectively (Ga–X and Ga–sodalite). The samples were washed and dried for 3 h at 110 °C, yielding 1.19 and 1.78 g of crystalline materials.

Sodium Ga–X gives an almost identical X-ray powder diffraction pattern to that of the aluminum analogue, 13-X.[10,11] The *d*-spacing values for the Ga–X are slightly larger than those for Na–X (13-X), which indicates a small expansion of structure upon replacing the aluminum with gallium.[10] The ^{29}Si NMR analysis of Ga–X indicates a Si/Ga mole ratio of 1.63. The X-ray powder pattern of Ga–sodalite is identical with the published data,[10] and indicates a small amount of the impurities, Ga–X zeolite and the Ga–analogue of the zeolite, natrolite. The ^{29}Si NMR analysis of Ga–sodalite indicates Si/Ga = 1.45. Both zeolites were dried in a drying pistol at 100 °C, under vacuum, over P_4O_{10}, for 12 h in order to remove residual $H_2{}^{17}O$.

Barium Exchange of [^{17}O] Gallosodalite. $BaCl_2$ (0.1 M, 10 mL) was heated to 50 °C, then 0.5 g of [^{17}O]gallosodalite was added. The slurry was stirred for 1 h at 50 °C, filtered, and washed. This procedure was then repeated two more times. The resultant Ba,Na-gallosodalite was dried at 100 °C for 12 h, yielding 0.45 g of partially exchanged material. Atomic absorption analysis indicated that the final composition is $Ba_{0.113}Na_{0.887}$ (mole ratio).

Synthesis of [^{17}O] $AlPO_4$-5.[12] Baker orthophosphoric acid (1.53 g) was mixed with 1.74 g of 50% ^{17}O-enriched water; then Al_2O_3 powder (0.92 g) was added and the mixture stirred to form a uniform slurry. Next, triethylamine (1.01 g) was added, with stirring, and the resultant gel loaded into a 25-mL Parr bomb. This was autoclaved at 200 °C for 27 h. The sample of $AlPO_4$-5 was washed, then dried for 1 h, yielding 1.30 g of crystalline material.

Synthesis of [^{17}O] $AlPO_4$-11.[12] Alfa orthophosphoric acid (0.77 g) and 2.0 g of 50% ^{17}O-enriched water were combined in a 25-mL Parr bomb liner. Al_2O_3 powder (0.46 g) was added, and the mixture was stirred until homogeneous. Next, dipropylamine (0.34 g) was added with stirring, and the resultant gel was autoclaved for 24 h at 200 °C, yielding 0.60 g of crystalline material.

Synthesis of [^{17}O] $AlPO_4$-17.[12] Alfa orthophosphoric acid (0.94 g) and 1.16 g of 50% ^{17}O-enriched water were mixed, and to this slurry was added 0.57 g of Al_2O_3; the mixture was stirred until homogeneous. Cyclohexylamine (0.41 g) was dissolved in 0.84 g of 50% ^{17}O-enriched water. This solution was added to the Al_2O_3/H_3PO_4 slurry, with stirring.

§This work was supported in part by DOE Grant No. DE-FG22-83PC60779, and in part by the U.S. National Science Foundation Solid-State Chemistry Program (Grant DMR 83-11339; G.L.T. and N.J.).

†University of Illinois at Urbana—Champaign.
‡Signal Research Center.

(1) Lippmaa, E.; Mägi, M.; Samoson, A.; Engelhardt, G.; Grimmer, A. R. *J. Am. Chem. Soc.* **1980**, *102*, 4889.
(2) Lippmaa, E.; Mägi, M.; Samoson, A.; Tarmak, M.; Engelhardt, G. *J. Am. Chem. Soc.* **1981**, *103*, 4992.
(3) Müller, D.; Jahn, E.; Fahlke, B.; Ladwig, G.; Haubenreisser, U. *Zeolites* **1985**, *5*, 53.
(4) Blackwell, C. S.; Patton, R. L. *J. Phys. Chem.* **1984**, *88*, 6135.
(5) Klinowski, J. *Prog. NMR Spectrosc.* **1984**, *16*, 237.
(6) Schramm, S.; Oldfield, E. *J. Am. Chem. Soc.* **1984**, *106*, 2502.
(7) Oldfield, E.; Kirkpatrick, R. J. *Science* **1985**, *227*, 1537.
(8) Timken, H. K. C.; Turner, G. L.; Gilson, J. P.; Welsh, L. B.; Oldfield, E. *J. Am. Chem. Soc.*, preceding paper in this issue.
(9) Vaughan, D. E. W.; Melchior, M. T.; Jacobson, A. J. *Intrazeolite Chemistry*; ACS Symposium Series No. 218; Stucky, G., Ed.; American Chemical Society: Washington, D.C., 1983; p 231.
(10) Selbin, J.; Mason, R. B. *J. Inorg. Nucl. Chem.* **1961**, *20*, 222.
(11) Argauer, R. J. U.S. Patent 3 431 219, 1969.
(12) Wilson, S. T.; Lok, B. M.; Flanigen, E. M. U.S. Patent 4 310 440, 1982.

0002-7863/86/1508-7236$01.50/0

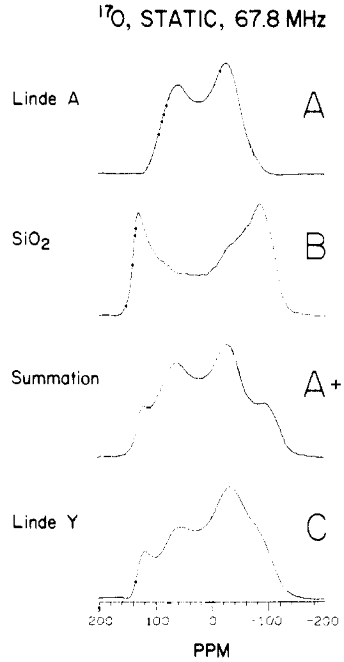

Figure 1. The 67.8 MHz (11.7 T) static ^{17}O NMR spectra of zeolites and low cristobalite (SiO_2): (A) [^{17}O]Na-A zeolite, 3599 scans, recycle time = 1 s; (B) [^{17}O] low cristobalite, 100 scans, recycle time = 120 s; (A + B) a simulated [^{17}O]Na-Y zeolite spectrum obtained by adding together the Na-A (Si-O-Al, A) and low cristobalite (Si-O-Si, B) spectra; (C) [^{17}O]Na-Y zeolite.

The resultant gel was autoclaved at 200 °C for 168 h, yielding 0.86 g of crystalline matterial.

Final calcination of these aluminophosphates were performed at 500 °C for 3 h, in order to remove organic templates and/or residual $H_2{}^{17}O$. The samples were characterized by X-ray powder diffraction and ^{27}Al and ^{31}P NMR.

Reagents used in the gallosilicate preparations were DuPont Ludox HS-40 colloidal silica, (40 wt. % SiO_2), gallium oxide (Aldrich, 99.99%), and Aldrich reagent grade sodium hydroxide. For the aluminophosphate syntheses we used Conoco Catapal SB alumina, (74.2 wt % Al_2O_3), orthophosphoric acid (Alfa ACS grade, 85%, or Baker reagent grade, 85.8%), triethylamine (Aldrich, 99%), dipropylamine (Aldrich, 99%), and cyclohexylamine (Aldrich, 97%). The ^{17}O-enriched water was obtained either from Cambridge Isotope Laboratories (20 atom % enrichment) or from Isotec (50 atom % enrichment).

Nuclear Magnetic Resonance Spectroscopy. ^{17}O NMR spectra were obtained on FT NMR spectrometers at 67.8 and 48.8 MHz, using Oxford Instruments (Osney Mead, Oxford, U.K.) 11.7 T (tesla), 52-mm bore or 8.45 T, 89-mm bore superconducting solenoid magnets, respectively. We used Nicolet Instrument Corp. (Madison, WI) Model-1280 computer systems for data acquisition, and Amplifier Research (Souderton, PA) Model 150LA and 200L amplifiers for final rf pulse generation. ^{17}O MASS NMR spectra at 11.7 T were obtained using a Doty probe (Doty Saientific, Columbia, SC) with spinning speeds of ≥6.5 kHz. Since the line widths are very broad for the aluminophosphates, relatively fast spinning speeds (≥6.5 kHz) were necessary in order to remove the spinning sidebands from the main peak. Static ^{17}O NMR spectra at both fields were obtained using a "home-built" horizontal solenoid-type sample probe. Chemical shifts are reported in parts per million from an external standard of tap water ($H_2{}^{17}O$, natural abundance). where more positive values correspond to low-field, high-frequency, paramagnetic or deshielded values (δ scale). Line broadenings due to exponential multiplication were 300 Hz for static and 50 Hz for MASS ^{17}O NMR spectra.

Experimental Results

We show in Figure 1 the static ^{17}O NMR spectra (at 67.8 MHz) of Na–A, low cristobalite, and Na–Y. To a first approximation, the spectrum of Na–Y (Figure 1C) may be simulated as the sum of the Na–A (Si–O–Al) and low cristobalite (Si–O–Si) spectra, as shown in Figure 1A,B. The assignment of the two chemically nonequivalent oxygens in Y zeolite is further supported by the intensity differences between the two spectral components as a function of Si/Al ratio.[8] For a given Si/Al or Si/Ga mole ratio (from the ^{29}Si MASS NMR spectrum), the relative intensities of the Si-O-Si fragment and the Si-O-Al or Si-O-Ga fragment can be calculated, based on the relation[8]

$$(\mathrm{Si/Al})\ \text{or}\ (\mathrm{Si/Ga}) = (0.5I_1 + 0.25I_2)/0.25I_2 \quad (1)$$

where I_1 is the percentage of Si-O-Si sites, I_2 is the percentage of Si-O-Al or Si-O-Ga sites, and $I_1 + I_2 = 100$.

We show in Figure 2A and 2E the 67.8-MHz static and MASS ^{17}O NMR spectra, respectively, of Na–Y zeolite, together with spectral simulations using the calculated relative intensities as estimated from eq 1. From the simulations we obtain the e^2qQ/h, η, and δ_i values, which are given in Table I and ref 8. As we discussed in the preceeding paper,[8] both the static and MASS NMR spectra reveal only chemically distinct oxygen components, Si[^{17}O]Si and Si[^{17}O]Al, as shown in the simulations, although the four crystallographically different oxygen sites may give a small distribution of observables. The same approach is used in order to interpret the static and MASS ^{17}O NMR spectra of the gallosilicates and aluminophosphates.

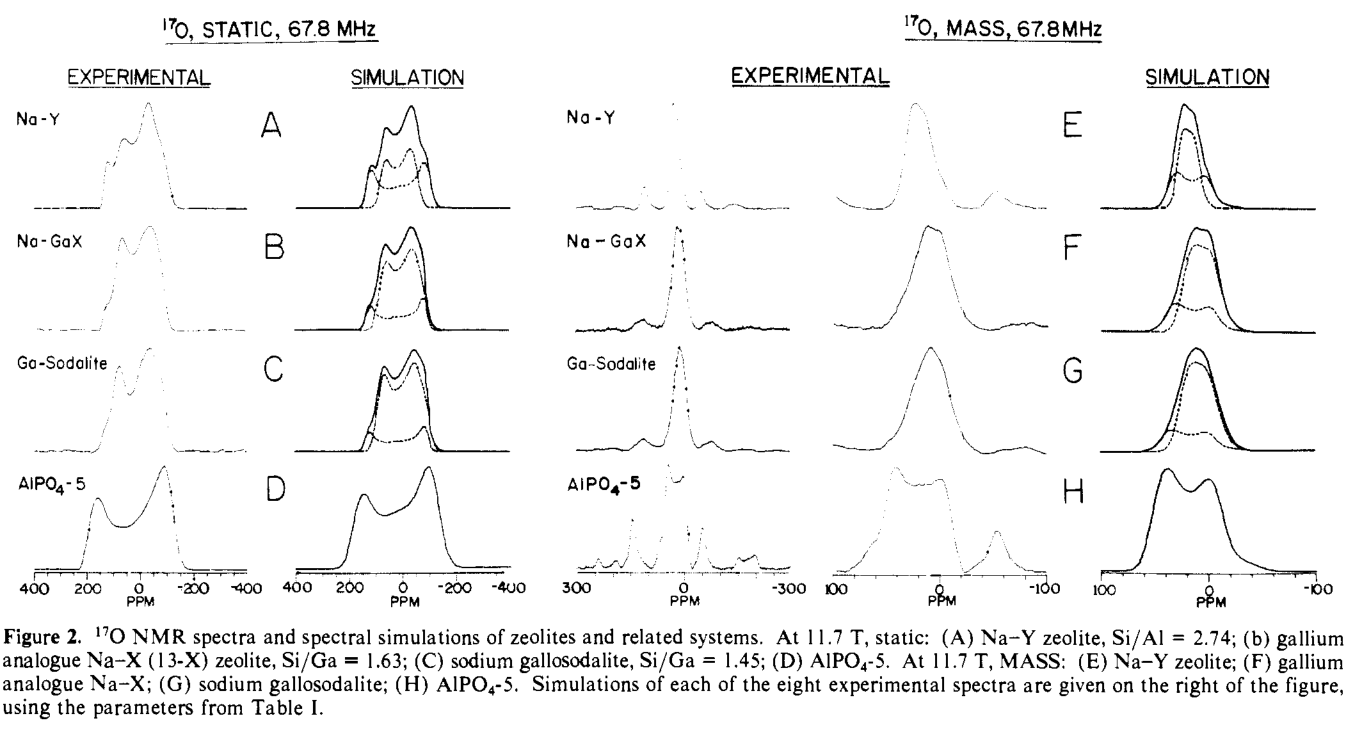

Figure 2. ^{17}O NMR spectra and spectral simulations of zeolites and related systems. At 11.7 T, static: (A) Na–Y zeolite, Si/Al = 2.74; (b) gallium analogue Na–X (13-X) zeolite, Si/Ga = 1.63; (C) sodium gallosodalite, Si/Ga = 1.45; (D) $AlPO_4$-5. At 11.7 T, MASS: (E) Na–Y zeolite; (F) gallium analogue Na–X; (G) sodium gallosodalite; (H) $AlPO_4$-5. Simulations of each of the eight experimental spectra are given on the right of the figure, using the parameters from Table I.

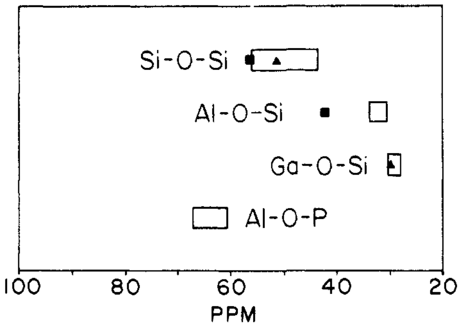

Figure 3. Isotropic chemical shift ranges for chemically distinct oxygen fragments in zeolites, and related systems. The squares correspond to the Na,Ba-Y zeolite and the triangles to the Na,Ba-gallosodalite.

We show in Figure 2B and 2F the static and MASS spectra of Ga-X zeolite with Si/Ga ratio of 1.63. From the simulations we obtain the e^2qQ/h, η, and δ_i values (Table I). As in the case of the ^{17}O NMR of zeolites A and Y,[8] there is a discrepancy in the e^2qQ/h values between static and MASS NMR, with the static values always being slightly larger than the MASS values. We believe this to be due to a chemical shift anisotropy effect, which is averaged out under MASS, although an orientation-dependent dipolar broadening may also contribute to the static results. Sodium gallosodalite, with Si/Ga mole ratio = 1.45, gives similar results, as shown in Figure 2C and 2G. MASS and static results are tabulated separately in Table I. These results indicate that the electronic structure around oxygen in the Si–O–Si fragment in gallosilicates is close to that in low cristobalite, while that in the Si–O–Ga fragment is more ionic, more shielded, and more asymmetric.

We show in Figure 2D the 67.8-MHz static NMR spectrum of a sample of the porous aluminophosphate, $AlPO_4$-5. The resonance consists of a broad second-order quadrupolar split doublet for the Al[^{17}O]P group, which can be characterized by e^2qQ/h = 6.5 MHz, η = 0.0, and δ_i = 63 ppm. Similarly, the MASS NMR spectrum (Figure 2H) yields no evidence for more than one oxygen site, and the spectrum is well simulated by e^2qQ/h = 5.7 MHz, η = 0.0, and δ_i = 61 ppm. The discrepancy in quadrupole coupling constants between static and MASS again probably arises because of the chemical shift anisotropy effect, which has not yet been included in our spectral simulation program. The other porous aluminophosphates, $AlPO_4$-11 and $AlPO_4$-17, also show a single, second-order quadrupole-split doublet for Al[^{17}O]P, and have very similar e^2qQ/h and δ_i parameters, as shown in Table I.

We show in Figure 3 a diagram of the isotropic chemical shift ranges for each fragment of oxygen in zeolites and $AlPO_4$ materials. In addition, the effect of nonframework cations on the ^{17}O chemical shift is shown for Ba^{2+}-exchanged gallosodalite and Y zeolite. It is apparent that for Ba–Y zeolite the chemical shifts of both Si–O–Al and Si–O–Si fragments are deshielded and that the deshielding is larger for the Si–O–Al fragment.[8] No similar deshielding effect was observed for the gallosodalite, presumably owing to the lower level of Ba^{2+} exchange. Further systematic studies of a variety of cation-exchanged zeolites and $AlPO_4$'s may provide insight into the nonframework cation dependence of the ^{17}O chemical shifts. Such studies may also provide information on the cation positions in such systems.

Theoretical Results

The electric field gradient (EFG) at a quadrupolar nucleus is extremely sensitive to the local electronic environment and to the details of bonding. For light atoms, such as ^{17}O, the EFG tensor is conveniently interpreted within the semiempirical framework proposed by Townes and Dailey,[13-16] wherein the EFG is ascribed

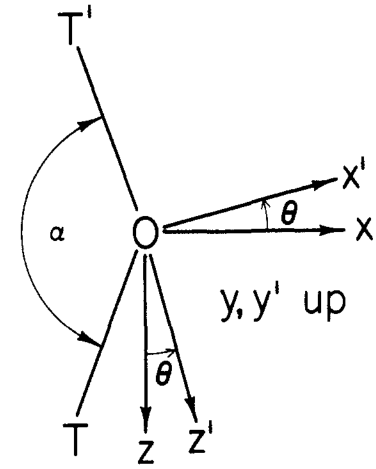

Figure 4. Axis system used in Townes–Dailey calculations. T and T' are in the x,z plane.

to an imbalance of the valence p-orbital occupations, assuming identical radial dependencies of the three 2p orbitals. The EFG tensor is dependent on the expectation value of the field gradient operator which is evaluated as follows, based on the Townes–Dailey (T–D) approximations, as described by Lucken:[14]

$$\begin{aligned}\int 2p_iH_i2p_i\,d\tau &= q_0\\ \int 2p_jH_i2p_j\,d\tau = \int 2p_kH_i2p_k\,d\tau &= -q_0/2\\ \int 2p_iH_{ij}2p_i\,d\tau = \int 2p_iH_{ij}2p_k\,d\tau &= 0\\ \int 2p_iH_{ij}2p_j\,d\tau &= (3/4)q_0\end{aligned} \quad (2)$$

H_i is the Hamiltonian for the electric field gradient along the i axis, and q_0 is the EFG produced by one unbalanced 2p electron, 20.88 MHz.[17]

The molecular orbitals, ψ_j, are expressed as a linear combination of oxygen atomic orbitals (LCAO):

$$\psi_j = \sum a_j\Phi_j \quad (3)$$

In the compounds of interest, oxygen exhibits a bridging angle greater than 120°, and the molecular orbitals are described using directed valence arguments by an sp^n ($1 \leq n \leq 2$) basis set, referenced to the molecular axis system shown in Figure 4:

$$\begin{aligned}\psi_1 &= p_y \qquad \psi_2 = \gamma_s + (1-\gamma^2)^{1/2}p_x\\ \psi_3 &= (1/\sqrt{2})[(1-\gamma^2)^{1/2}s - \gamma p_x + p_z]\\ \psi_4 &= (1/\sqrt{2})[(1-\gamma^2)^{1/2}s - \gamma p_x - p_z]\end{aligned} \quad (4)$$

where $\gamma = \cot(\alpha/2)$. The matrix elements of the EFG tensor are solved using the approximations from eq 2 and 3 as follows:[14]

$$\begin{aligned}q_{ii}/q_0 &= \sum_{l=1}^{4} n_l[a_{li}^2 - \tfrac{1}{2}(a_{lj}^2 + a_{lk}^2)]\\ q_{ij}/q_0 &= (3/2)\sum_{l=1}^{4} n_l a_{li} a_{lj} \qquad (i \neq j)\end{aligned} \quad (5)$$

where n_l represents the orbital occupancy of the ψ_l orbital. The EFG tensor in the molecular axis system is evaluated using eq 4 and 5.

$$\begin{aligned}q_{xx}/q_0 &= -n_1/2 + n_2(1-\gamma^2) + (1/4)(n_3+n_4)(2\gamma^2-1)\\ q_{yy}/q_0 &= n_1 - (n_2/2)(1-\gamma^2) - (1/4)(n_3+n_4)(\gamma^2+1)\\ q_{zz}/q_0 &= -n_1/2 - (n_2/2)(1-\gamma^2) + (1/4)(n_3+n_4)(2-\gamma^2)\\ q_{xz}/q_0 &= (3/4)(n_4-n_3)\gamma \qquad q_{xy} = q_{yz} = q_{yx} = q_{zy} = 0\end{aligned} \quad (6)$$

(13) Townes, C. H.; Dailey, B. P. *J. Chem. Phys.* **1949**, *17*, 782.
(14) Lucken, E. A. C. *Nuclear Quadrupole Coupling Constants*; Academic Press: New York, 1969.
(15) Janes, N.; Oldfield, E. *J. Am. Chem. Soc.* **1986**, *108*, 5743.
(16) Woyciesjes, P. M.; Janes, N.; Ganapathy, S.; Hiyama, Y.; Brown, T. L.; Oldfield, E. *Magn. Reson. Chem.* **1985**, *23*, 315.
(17) Harvey, J. S. M. *Proc. R. Soc. London, Ser. A* **1965**, *285*, 581.

For the symmetric T–O–T linkage ($n_4 = n_3$), the off-diagonal term is zero and the molecular axis system described above coincides with the principal axis system. In general, however, $n_3 \neq n_4$ and the matrix must be diagonalized by a rotation of θ in the xz plane as shown in Figure 4, and we obtain eq 7.

$$q_{x'x'} = q_{xx}\cos^2\theta - 2q_{xz}\sin\theta\cos\theta + q_{zz}\sin^2\theta \qquad q_{y'y'} = q_{yy}$$
$$q_{z'z'} = q_{xx}\sin^2\theta + 2q_{xz}\cos\theta\sin\theta + q_{zz}\cos^2\theta$$
$$q_{z'x'} = q_{x'z'} = (q_{xx} - q_{zz})\sin\theta\cos\theta + q_{xz}(\cos^2\theta - \sin^2\theta) \quad (7)$$
$$q_{x'y'} = q_{y'x'} = q_{y'z'} = q_{z'y'} = 0$$

The EFG matrix becomes the principal axis system if the off-diagonal term vanishes so that

$$\tan 2\theta = 2q_{xz}/(q_{zz} - q_{xx}) \quad (8)$$

and the EFG components in the principal axis system become:

$$q_{z'z'} = (q_{xx}/2)(1 - \sec 2\theta) + (q_{zz}/2)(1 + \sec 2\theta)$$
$$q_{y'y'} = q_{yy} \quad (9)$$
$$q_{x'x'} = (q_{xx}/2)(1 + \sec 2\theta) + (q_{zz}/2)(1 - \sec 2\theta)$$

The interaction of the field gradient, eq, and the nuclear quadrupole moment, eQ, gives rise to the NMR observables e^2Qq/h and η. By definition

$$|e^2Qq_{ZZ}| \geq |e^2Qq_{YY}| \geq |e^2Qq_{XX}| \quad (10)$$

and

$$\eta = \frac{e^2Qq_{XX} - e^2Qq_{YY}}{e^2Qq_{ZZ}} \quad (11)$$

Previously, we have analyzed the ^{17}O e^2qQ/h of the symmetric Si–O–Si linkage, and reported that the major principal axis (e^2Qq_{ZZ}) lies in the Si–O–Si plane, perpendicular to the bisector of the bridging angle (along the z axis in Figure 4).[15] Using the convention above and eq 6 and 9, expressions for the NMR observables in terms of orbital occupations are obtained in eq 12.

$$\tan 2\theta = [(n_3 - n_4)\tan\alpha]/(n_3 + n_4 - 2n_2)$$
$$e^2Qq_{ZZ}/h = [(-1/2)n_1 + (n_2/4)(1 - \gamma^2) + ((n_3 + n_4)/8)(1 + \gamma^2) + \sec 2\theta[-(3/4)n_2(1 - \gamma^2) + (3/8)(n_3 + n_4)(1 - \gamma^2)]]e^2Qq_0/h$$
$$(e^2Qq_{ZZ}/h)(1 + \eta) = [-2n_1 + n_2(1 - \gamma^2) + (1/2)(n_3 + n_4)(1 + \gamma^2)]e^2Qq_0/h$$
$$(e^2Qq_{ZZ}/h)(3 - \eta) = (3(n_4 - n_3)\gamma/\sin 2\theta)e^2Qq_0/h \quad (12)$$

These equations contain four unknowns (the four orbital occupancies) and only two knowns (the NMR observables) and, consequently, cannot be solved directly.

In the case of low cristobalite (SiO_2), however, $n_3 = n_4$, and the oxygen effective atomic charge is known to satisfy electroneutrality (–0.5 eu),[18] so that there are three unknowns and three knowns. Using the MASS values for SiO_2, $e^2Qq/h = 5.3$ MHz and $\eta = 0$, we obtain the following orbital occupancies: $n_3 = n_4 = 1.4906$, $n_1 = 1.7444$, and $n_2 = 1.7744$. As we have noted previously, these values are in excellent agreement with Pauling's model of a 50% ionic Si–O bond with a bond order of 1.55.[15]

In the case of the asymmetric linkage, however, we are unable to solve for the four unknown orbital occupations, or the three differences in orbital occupations, on the basis of the two NMR observables. Nonetheless, it is instructive to introduce certain simplifications which allow the development of a framework in which to discuss the experimental results. Therefore, we shall assume that the major difference between the Si–O–Si and T–O–T′ linkages involves the ionic character of the σ bonds. We choose to calculate these orbital occupations, n_3 and n_4, using Pauling's thermochemical electronegativities and ionic character relation,[19] which we have previously shown gives reasonably good agreement with the T–D method in reproducing the experimental e^2qQ/h of a number of bicoordinate oxygen compounds.[15] While approximate, we expect, at the very least, the proper ordering of the e^2qQ/h values.

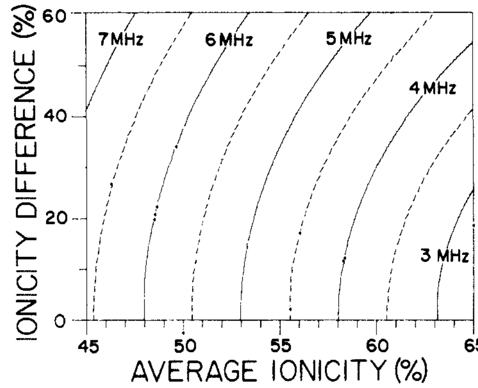

Figure 5. Expected dependence of e^2qQ/h shown as contours, on varying the ionicities of the tetrahedral cations in the T–O–T′ linkage. Ionicities are calculated from Pauling's relations.[19] The abscissa is empirically shifted slightly so that the observed average ionicity of cristobalite (49.1%) coincides with Pauling's prediction (51.4%).

The results of varying the ionicity of the cristobalite-like T–O–T′ linkage is shown in Figure 5, presented as contours of e^2qQ/h, as a function of the average ionicity and the difference in ionicity of the tetrahedral cations. For instance, the Al–O–P linkage in $AlPO_4$-n is characterized by an O–Al bond, 63.21% ionic, and an O–P bond, 38.74% ionic, leading to an average ionicity of 50.98% and a difference in ionicity of 24.47%. On this basis, a e^2qQ/h of –5.58 MHz is predicted for a typical Al–O–P linkage, which is very close to the experimental value (from MASS) of 5.6–5.7 MHz (Table I).

Generally, we expect that more ionic linkages will exhibit smaller e^2qQ/h, while increasing the asymmetry for a given average ionicity will result in an increased e^2qQ/h. The major EFG component, q_{ZZ}, is perpendicular to the bisector of the bridging angle for the symmetric linkage, and is rotated in the T–O–T′ plane toward the more covalent tetrahedral cation T′–O axis as the difference in the ionicities increases.

The e^2qQ/h is more sensitive to the difference in ionicity at bridging angles near 120° (not shown), and becomes insensitive to such changes at a linear bridging angle, since q_{ZZ} remains fixed along the T–O–T′ axis, regardless of ionicity difference, for sp hybridization.

Of course, not all oxygen linkages can be modeled by varying the σ bonding orbital ionicities of a cristobalite structure. Changes in coordination number, bridging angle, and degree of π-back-bonding all affect the e^2qQ/h. Thus, in order to use Figure 5 interpretively, its limitations must be recognized. First, the predictions concern only *bicoordinate* oxygen compounds. We have used the Townes–Dailey model previously to discuss the effect of coordination on the e^2qQ/h of bridging oxygens.[15] A significantly smaller e^2qQ/h was obtained for the tetracoordinate (2Si, 2Ca) bridging oxygen of the chain silicate diopside, $CaMgSi_2O_6$, than was observed for the bicoordinate (2Si) bridging oxygen of low cristobalite. The observed decrease in e^2qQ/h from 5.3 to 4.3 MHz (MASS) was ascribed as largely due to the additional coordination in the chain silicate. Therefore, *we expect that nonframework cation coordination to bridging oxygen will result in a smaller e^2qQ/h than that predicted* from Figure 5.

Second, we have assumed that the degree of π-back-bonding remains constant. While this may be reasonable for the elements of the third row, we expect that such effects may be smaller for heavier elements. In previous work[15] we have shown that a decrease in π-back-bonding will result in a larger e^2qQ/h than that predicted from Figure 5. This effect should be significant if none

(18) LePage, Y.; Donnay, G. *Acta Crystallogr., Sect. B: Struct. Sci.* **1976**, *32*, 2456.

(19) Pauling, L. *The Nature of the Chemical Bond*; Cornell University Press: Ithaca, 1960.

Table I. ^{17}O Nuclear Quadrupole Coupling Constants (e^2qQ/h), Electric Field Gradient Tensor Asymmetry Parameter (η), and Isotropic Chemical Shifts (δ_i) for Zeolites and Related Systems[a]

		static			MASS		
system	fragment	e^2qQ/h (MHz)	η	δ_i (ppm, H_2O)	e^2qQ/h (MHz)	η	δ_i (ppm, H_2O)
Na-A	Si-O-Al	4.2 (3.8)	0.2 (0.2)	33 (32)	3.2	0.2	32
Na-Y	Si-O-Al (53.5)[b]	4.2 (4.0)	0.2 (0.2)	31 (32)	3.1	0.2	31
	Si-O-Si (46.5)[b]	5.7 (5.3)	0.1 (0.1)	46 (48)	4.6	0.1	44
SiO_2	Si-O-Si	5.8	0.0	46	5.3	0.0	44
Ba,Na-Y	Si-O-Al (53.5)[b]	4.0	0.2	45	3.4	0.4	40
	Si-O-Si (46.5)[b]	5.6	0.1	57	5.1	0.15	52
Ga-X	Si-O-Ga (76.0)[b]	4.6 (4.3)	0.3 (0.3)	28 (29)	4.0	0.3	28
	Si-O-Si (24.0)[b]	5.6 (5.5)	0.0 (0.0)	50 (50)	5.0	0.0	49
Ga-sodalite	Si-O-Ga (81.6)[b]	4.8 (4.3)	0.3 (0.35)	29 (31)	4.0	0.3	29
	Si-O-Si (18.4)[b]	5.7 (5.5)	0.0 (0.0)	52 (49)	5.1	0.0	51
Na,Ba	Si-O-Ga (81.6)[b]	4.8	0.3	29	4.0	0.3	29
Ga-sodalite	Si-O-Si (18.4)[b]	5.7	0.0	52	5.1	0.0	51
$AlPO_4$-5	Al-O-P	6.5 (6.2)	0.0 (0.0)	63 (62)	5.7	0.0	61
$AlPO_4$-11	Al-O-P	6.4 (6.2)	0.0 (0.0)	64 (63)	5.7	0.0	63
$AlPO_4$-17	Al-O-P	6.3 (6.15)	0.1 (0.0)	67 (63)	5.6	0.0	63

[a] At 11.7 T. Values at 8.45 T are given in parentheses. [b] Calculated percentage contributions for each fragment from the Si/Al or Si/Ga mole ratios.

of the tetrahedral cations are Al, Si, or P. For similar reasons, we restrict our attention to the linkage of *tetrahedral* cations. For example, trigonal boron is likely to accept a greater degree of π-back-bonding into the vacant boron π orbital, thus causing a lower e^2qQ/h than that predicted from this simple model.

Third, we have chosen a constant bridging angle of 144° (the average in SiO_2 polymorphs) to obtain the results in Figure 5. As we have discussed in previous work,[15] the dependence of the e^2qQ/h on bridging angle is of great interest regarding the origins of the bond-length–bridging-angle correlation observed for silicates. To date, however, this dependence has not been characterized. Semiempirical calculations for different bonding models suggest that the dependence is modest, but uncertainties of hundreds of kilohertz are not unexpected.[15] Preliminary experimental results suggest that this dependence is indeed secondary. We have been unable to resolve oxygen sites which differ with respect to bond angle either on the basis of e^2qQ/h or chemical shift as indicated by our ability to simulate the spectra using a single component with good success. Thus preliminary results suggest that the dependence of the chemical shift and e^2qQ/h on bridging angle is small; however, further work is necessary in order to clarify this point. From a practical standpoint, however, we expect that based on an intermediate bridging angle, the model will yield reasonable e^2qQ/h values, for a given T–O–T′ linkage.

Lastly, there are uncertainties within the LCAO approach. Since the local C_{2v} symmetry is broken in the asymmetric linkage, the hybridization character of the oxygen σ bonding orbitals (n_3, n_4) may differ slightly. Indeed small differences in hybridization (and in turn orbital electronegativity) have been postulated with reference to the silicon-29 NMR chemical shift.[20] Furthermore, distortions of the LCAO basis set induced by lattice charges have been neglected. Previously, we have had good success with the T–D model used with Pauling ionicities in reproducing the e^2qQ/h of a variety of bicoordinate compounds; however, we caution that lattice effects are likely to become increasingly important for the more ionic linkages.

Discussion

The experimental results and theoretical predictions based on the Townes–Dailey approach are shown in Tables I and II. We regard the values obtained from the MASS experiment as more accurate, since MASS averages the chemical shift anisotropy. The e^2qQ/h values predicted from the simplified T–D analysis are in good agreement with experiment in reproducing the proper ordering of the e^2qQ/h (Al–O–P > Si–O–Si > Ga–O–Si > Al–O–Si). The predicted value for Al–O–P is in good agreement with experiment. The model, however, predicts a slightly larger e^2qQ/h for both the Ga–O–Si and Al–O–Si linkages than observed. Given the substantial simplifications involved in the model, we are nevertheless quite satisfied that the correct ordering of the experimental e^2qQ/h is reproduced. However, it is instructive to seek a chemical rationale for the lower e^2qQ/h observed experimentally for the Ga–O–Si and Al–O–Si linkages. As mentioned previously, one factor decreasing the e^2qQ/h from the value predicted in Figure 5 is coordination to nonframework cations. In diopside, a 1-MHz decrease was observed for cation coordinated oxygen with respect to the framework oxygen linkage; this was attributed to calcium coordination. Similarly, both the Ga–O–Si and Al–O–Si linkages exhibit experimental e^2qQ/h (MASS)

Table II. ^{17}O Nuclear Quadrupole Coupling Constants (e^2qQ/h) and Asymmetry Parameter (η) Predicted for Bicoordinate Linkages[a]

fragment	e^2qQ/h predicted	η predicted
Si-O-Si	−5.30	0.00
Si-O-Al	−4.19	0.06[b]
Si-O-Ga	−4.53	−0.13[b]
Si-O-Ge	−5.30	0.00
Al-O-P	−5.58	−0.03[b]
Si-O-B[c]	−6.40	0.02
Al-O-Ge	−4.20	0.06[b]
Ga-O-P	−5.89	−0.01[b]
B-O-P[c]	−7.63	0.05

[a] Model as described in text. [b] For η positive, using notation in Figure 4, $|q_{z'z'}| \geq |q_{y'y'}| \geq |q_{x'x'}|$. For η negative, $|q_{z'z'}| \geq |q_{x'x'}| \geq |q_{y'y'}|$. [c] Tetrahedral boron only.

Table III. Comparison between Experimental and Predicted ^{17}O Nuclear Quadrupole Coupling Constants

		T–D method[b]		Schramm and Oldfield[c]	
fragment	e^2qQ/h (MHz, exptl)[a]	prediction	% dev[d]	prediction	% dev[d]
Si-O-Si	5.02[e]	−5.30	−5.6	4.4	12.4
Si-O-Al	3.18[f]	−4.19	−31.8	3.2	−0.6
Si-O-Ga	4.0[g]	−4.53	−13.3	3.6	10.0
Al-O-P	5.67[h]	−5.58	1.6	4.4	22.4

[a] Obtained from simulation of 67.8 MHz (11.7 T) MASS NMR experiment; accuracy is ±5%. [b] Obtained from the Townes–Dailey calculation described in the text; assumed bicoordinate bridging oxygen and SiO_2 (cristobalite) structure. [c] Obtained from the mean ionicity of the A–O and O–B bonds as described in ref 6, using EN O = 3.5, EN Al = 1.5, EN Si = 1.8, EN P = 2.1, and EN Ga = 1.6. [d] Deviation = [(experimental − |predicted|)/experimental] × 100, in percent. [e] Averaged value of Si–O–Si in Na-Y, NH_4-Y (Si/Al = 2.92, 4.98, and 7.51), dealuminated Na-Y, SiO_2 (low cristobalite), Na-GaX, and sodium gallosodalite. [f] Averaged value of Si–O–Al in Na-A, Na-Y, and the three NH_4-Y zeolites. [g] Averaged value of Si–O–Ga in Na-GaX and sodium gallosodalite. [h] Averaged value of Al–O–P in $AlPO_4$-5, $AlPO_4$-11, and $AlPO_4$-17.

(20) Radeglia, R.; Engelhardt, G. *Chem. Phys. Lett.* **1985**, *114*, 28.

values approximately 0.5 and 1 MHz, respectively, lower than expected. This implies, we believe, that the large majority of these sites are coordinated to nonframework cations. Certainly, in Na–A zeolite (Si/Al = 1), we expect that the vast majority of the linkages will exhibit coordination to sodium.

Pauling's rules predict that the nonframework cations should preferentially coordinate to the Al–O–Si and Ga–O–Si linkages over the Si–O–Si linkage.[19] The nearly identical e^2qQ/h, η, and δ_i observed for the Si–O–Al linkage in Na–A and Na–Y suggest that the local electronic environment of this oxygen is quite similar in both cases, and, within our resolution, coordinated to nonframework cations. Although we have not yet detected uncoordinated Al–O–Si and Ga–O–Si linkages, we expect their e^2qQ/h values to be larger than those of coordinated species. The results for the Si–O–Si linkage in Na–Y are more ambiguous. The static e^2qQ/h is similar to the framework Si–O–Si linkage in low cristobalite, but the MASS value is intermediate to that expected for nonframework cation coordinate and the strictly bicoordinate species. As an independent check, therefore, we have made the barium-exchanged species. Large group 2 nonframework cations tend to shift the oxygen resonances to more deshielded values.[21] We observe a change in the chemical shift of both the Si–O–Si and Si–O–Al linkages (still, Al–O–Si has a more deshielded chemical shift), thereby suggesting that both linkages may be coordinated, at least in the barium variant of Y zeolite.

In the gallosilicates, the e^2qQ/h values for Si–O–Si linkage for all of the species are similar to that found in low cristobalite, in both the MASS and static cases. This would tend to indicate that the nonframework cations are preferentially coordinated to the Si–O–Ga linkage at the expense of the Si–O–Si linkage.

Finally, presented in Table III is a comparison between the experimentally observed average ^{17}O e^2qQ/h values for Si[^{17}O]Si, Si[^{17}O]Al, Si[^{17}O]Ga, and Al[^{17}O]P, and those prediced by the Townes–Dailey analysis presented in this publication, and from the wholly empirical correlation presented previously.[6] Although more systems should clearly be studied to firmly establish such trends, we believe that the results of Table III strongly suggest, for purely bicoordinate oxygen linkage (Si–O–Si, Al–O–P), that the T–D analysis is more reliable, while in systems having additional nonframework cation coordination, that use of the empirical correlation is most appropriate.

Acknowledgment. This publication was prepared with the support of the U.S. DOE Office of Fossil Energy Grant No. DE-FG22-83PC60779. However, any opinions, findings, conclusions, or recommendations expressed herein are those of the authors and do not necessarily reflect the views of the Department of Energy.

(21) Turner, G. L.; Chung, S. E.; Oldfield, E. *J. Magn. Reson.* **1985**, *64*, 316.

Factors Influencing the C=N Stretching Frequency in Neutral and Protonated Schiff's Bases

J. J. López-Garriga, G. T. Babcock,* and J. F. Harrison*

Contribution from the Department of Chemistry, Michigan State University, East Lansing, Michigan 48824-1322. *Received September 12, 1985*

Abstract: The C=N stretching frequency has been studied in a series of aromatic Schiff's bases, their protonated derivatives, and their reaction products with other Lewis acids. Protonation, deuteration, or reaction with BF_3 increases the C=N stretching frequency in a range from 1 to 80 cm^{-1}. Linear polyene Schiff's bases show similar behavior: an increase in the C=N frequency of ~30 cm^{-1} is observed upon complexation of *trans*-retinal Schiff's base by BF_3. The magnitude of the increase in the C=N vibrational mode is dependent on the extent of conjugation in the aromatic system, on the nature of the substituent, and on the strength of the Lewis acid. In the NMR spectra of the protonated or complexed species a downfield chemical shift of the protons nearby the C=N bond is observed which suggests that the nitrogen electronegativity increases in the reaction product relative to the free Schiff's base. These observations, plus the similarities in behavior of Schiff's bases and nitriles, suggest that rehybridization at the Schiff's base nitrogen occurs on reaction of its lone pair with Lewis acids to increase the C=N bond order. Ab initio calculations on the Schiff's base, methylimine (see following paper), support this idea as the C=N bond length decreases and the C=N stretching force constant increases by 0.51 mdyn/Å upon protonation. Normal coordinate analysis of this species, of the model structure, $CH_3HC{=}NCH_3$, and of their protonated and deuterated derivatives are reported here which show that an increase in the stretching force constant of this magnitude leads to an increase of ~30 cm^{-1} in the frequency of the C=N stretching vibration. Analogous normal coordinate calculations were also carried out for the BF_3 addition product which show that a similar increase in C=N stretching force constant upon complexation is likely. The results indicate that rehybridization effects, in particular, an increase in the s orbital contribution from the protonated nitrogen to the sp^2 hybrid orbital in the Schiff's base linkage, are primarily responsible for the increase in the C=N stretching frequency upon complexation of a Schiff's base by a Lewis acid.

Schiff's base (**1**) and protonated Schiff's base (**2**) C=N vibrational modes have been studied for at least the past three decades.[1] Part of the interest in these species derives from the

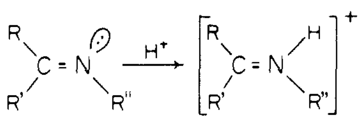

1 2

observation of functionally significant Schiff's base linkages in biological systems, for example, in pyridoxal enzymes[2] and, more recently, in rhodopsin, bacteriorhodopsin, and related visual cycle intermediates and models.[3] In rhodopsin, the retinal chromophore

(1) (a) Fabian, M. J.; Legrand, M.; Poirier, P. *Bull. Soc. Chim. Fr.* **1956**, 1499–1509. (b) Fabian, M. J.; Legrand, M. *Ibid.* **1956**, 1641–1643.

(2) (a) Witkop, B.; Beiler, T. W. *J. Am. Chem. Soc.* **1954**, *76*, 5589–5597. (b) Karube, Y.; Ono, Y.: Matsushima, Y.; Ueda, Y. *Chem. Pharm. Bull.* **1978**, *26*, 2642–2648. (c) Ledbetter, J. W. *J. Phys. Chem.* **1982**, *86*, 2449–2451. (d) Benecky, M. J.; Copeland, R. A.; Hayes, T. R.: Lobenstine, E. W.; Rava, R. P.; Pascal, R. A., Jr.; Spiro, T. G. *J. Biol. Chem.* **1985**, *260*, 11663–11670. (e) Benecky, M. J.; Copeland, R. A.; Rava, R. P.; Feldhaus, R.; Scott, R. D.; Metzler, C. M.; Metzler, D. E.; Spiro, G. T. *Ibid.* **1985**, *260*, 11671–11678.

0002-7863/86/1508-7241$01.50/0